JOURNAL OF ELECTROMAGNETIC ENGINEERING AND SCIENCE, VOL. 26, NO. 1, 39~48, JAN. 2026

https://doi.org/10.26866/jees.2026.1.r.338
ISSN 2671-7263 (Online) · ISSN 2671-7255 (Print)

Impedance-Modulating Patch Integration for Gain and Bandwidth Control of Antenna-in-Display in Millimeter-Wave Smartphones

Byeongjin Kim · Jeongtaek Oh · Kiseo Kim · Jungsuek Oh*

Abstract

In this study, an impedance-modulating patch (IMP) antenna-in-display (AiD) scheme is introduced to enable on-demand modification of the antenna operating frequency, bandwidth, and gain by selectively laminating a film with a printed IMP onto a pre-designed AiD. By adjusting the integration position of the IMP over the AiD folded dipole antenna, the gain and bandwidth are easily modified to meet the desired antenna characteristics. This approach facilitates flexible antenna performance while retaining the advantages of AiD without having to reproduce the entire mask for the mother glass, thereby avoiding excessive costs that display manufacturers typically seek to minimize. Two design examples are presented: a wideband version with a 28% bandwidth and a high-gain version achieving 6.25 dBi. The latter is validated through measurement. IMP-AiD thus offers a practical solution for next-generation display antennas.

Key Words: Antenna-in-Display (AiD), Bandwidth Control, Display Antenna, Gain Control, Impedance-Modulating Patch (IMP).

I. Introduction

Global IT companies have recently launched new smartphone models capable of 5G wireless communication using millimeter-wave (mmWave) frequency bands. These mmWave 5G smartphones typically include two or three antenna-in-package modules positioned in the backplane of the motherboard or the side bezel area to enable 5G communication with wide beam coverage [1–4].

To further expand the antenna space and beam coverage, a new antenna concept called antenna-on-display (AoD) has been proposed. In AoD, antennas are integrated into the front glass of smartphones and other display-equipped devices [5–9], as shown in Fig. 1(b). Notably, since AoD patch antennas are usually stacked on the OLED panel, they are composed of optically transparent conductors (TCOs) to maintain invisibility. Typical TCOs are mesh-grid metal patterns [10–13] or transparent conductive materials, such as indium tin oxide [14, 15]. However, AoD antennas suffer from low radiation efficiency owing to the high conductor loss of TCOs, which are used for both radiators and feedlines [8]. Additionally, the complex OLED panel, which can be considered an imperfect PEC ground, further degrades antenna performance.

Following the introduction of AoD, another display antenna concept termed antenna-in-display (AiD) was proposed [16, 17]. Unlike AoD, the radiator of an AiD folded dipole antenna (FDA) is embedded within the invisible dead space (DS) at the edge of the OLED panel. This placement allows the radiator and feedline to be composed of opaque solid conductors, which

Manuscript received January 23, 2025 ; Revised April 15, 2025 ; Accepted June 24, 2025. (ID No. 20250123-012J)
Institute of New Media and Communications, Electrical and Computer Engineering, Seoul National University, Seoul, Korea.
*Corresponding Author: Jungsuek Oh (e-mail: jungsuek@snu.ac.kr)

have significantly lower resistivity. As a result, AiD antennas usually achieve higher radiation efficiency than AoD patch antennas. AiD involves integrating the FDA design into the OLED panel fabrication process, thus eliminating the significant bonding loss of up to 4 dB that occurs in the case of AoD when the short-feedline-printed antenna film and the prolonged-feedline-printed FPCB are conductively bonded [5].

However, while integrating the AiD FDA into the OLED panel during the latter's fabrication process is beneficial, it limits the versatility of AiD characteristics. The AiD FDA and its feedline are printed simultaneously with the OLED panel when the latter is mass-printed onto the large mother glass using a mask. This implies that to modify antenna characteristics, such as frequency, bandwidth, or gain, the entire mask for the mother glass must be reproduced, incurring excessive costs that display manufacturers seek to avoid.

In this paper, we propose a novel display antenna concept—the impedance-modulating patch-integrated AiD (IMP-AiD)—that involves laminating a parasitic patch onto the AiD FDA (as shown in Fig. 1) at different positions to control the frequency, bandwidth, and gain of the pre-determined AiD FDA design. Two types of IMP-AiDs are demonstrated: Ver. 1, which exhibits wideband operation, and Ver. 2, which offers a high gain. The simulation and measurement results confirm the validity of the proposed display antenna concept.

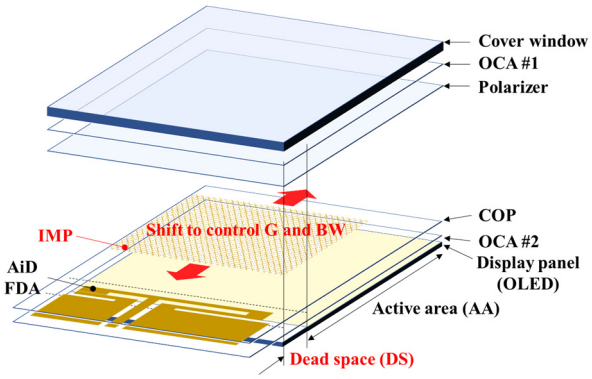

(a)

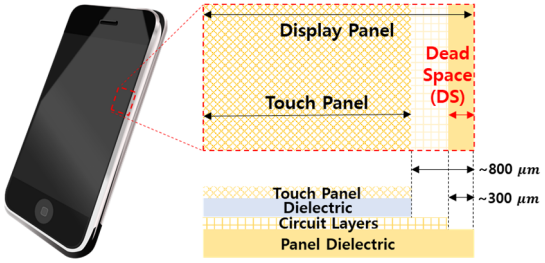

(b)

Fig. 1. Illustration of (a) the proposed IMP-AiD scheme and (b) the dead space at the edge of the OLED display panel (top view and vertical view).

II. IMP-AiD Configuration

Figs. 1 and 2 illustrate the configuration of the proposed IMP-AiD scheme. The dielectric constant (ϵ_r) and thickness (h) of the cover window, optically clear adhesives (OCA) #1 and #2, polarizer, and cyclo-olefin polymer (COP) film are as follows:

(1) Dielectric constant: ($\epsilon_{r,window}$, $\epsilon_{r,OCA1}$, $\epsilon_{r,OCA2}$, $\epsilon_{r,polarizer}$, $\epsilon_{r,COP}$) = (6.9, 2.58, 2.58, 2.92, 2.33)

(2) Thickness (in mm): (h_{window}, h_{OCA1}, h_{OCA2}, $h_{polarizer}$, h_{COP}) = (0.48, 0.15, 0.025, 0.104, 0.1)

The dipole antenna—AiD FDA—is integrated into the DS,

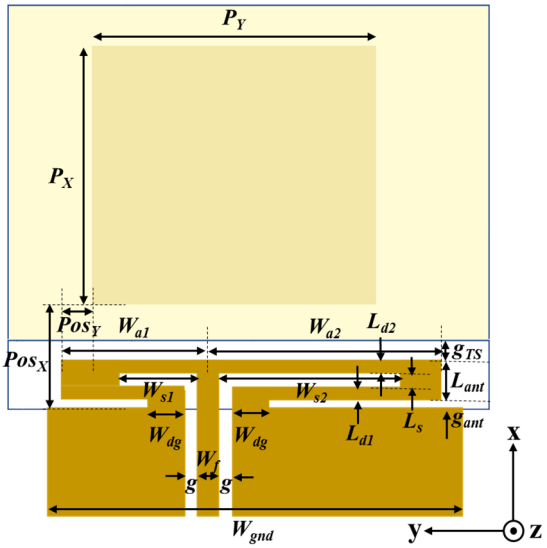

(a)

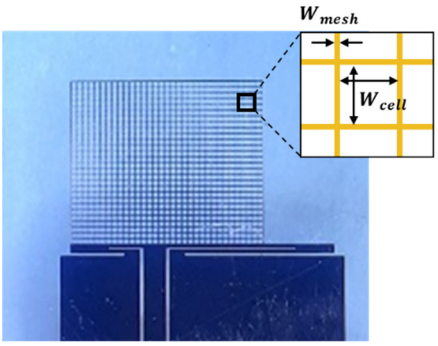

(b)

Fig. 2. (a) Configuration of the IMP-AiD and its parameters. The fixed parameters and their assigned values are: W_{gnd}=5.4, W_f=0.445, g=0.054, W_{dg}=0.3, W_{a1}=1.425, W_{a2}=3.225, W_{s1}=0.454, W_{s2}=2.254, L_{d1}=0.04, L_{d2}=0.05, L_s=0.06, g_{ant}=0.1, g_{TS}=0.05, L_{ant}=0.15 (unit: mm). The variable parameters for gain and bandwidth control of the AiD FDA are (P_X, P_Y, Pos_X, Pos_Y); (b) Photograph of the fabricated sample with the variable parameters set to (P_X, P_Y, Pos_X, Pos_Y)=(3,3.4,0.1,0) (unit: mm). W_{cell} and W_{mesh} are 0.09 mm and 0.01 mm, respectively.

which is the 300-μm-wide edge of the OLED panel, with the invisible patch (IMP) stacked on top of the FDA. Although the AiD FDA should ideally be embedded within the OLED panel during panel fabrication, doing so would incur unnecessarily high costs for fabricating benchtop samples during the testing stage. To address this, we fabricated a benchtop sample that closely resembled the original concept. In this setup, the IMP and FDA were printed on the top and bottom surfaces of the COP film, respectively, using 500-nm-thick copper. The assembly was affixed to the OLED display panel using an ultrathin OCA layer, which was only 25 μm thick. Simulations [16] confirmed that the 25 μm vertical displacement of the FDA had a minimal effect on the antenna's performance. From this point onward, the values assigned to the FDA design parameters were kept fixed since the primary objective of this paper is to modify only the IMP design parameters to control the gain and bandwidth of the OLED-integrated AiD FDA. Consequently, this paper presents parametric studies conducted on the IMP, while those related to the FDA are not included. Moreover, additional details on how the various antenna parameter values were determined can be found in our previous paper [16]. The fixed FDA design parameters and their corresponding values are provided in Fig. 2(a), while the variable parameters for the IMP are P_X, P_Y, Pos_X, and Pos_Y. Notably, the IMP and FDA overlap when Pos_X is less than 0.25 mm in the top view depicted in Fig. 2(a) because they are located in different layers. Fig. 2(b) shows a photograph of the fabricated sample to facilitate better understanding.

III. Ver. 1: Wideband IMP-AiD Design

The variable parameters for the designed wideband IMP-AiD Ver. 1 were set to $(P_X, P_Y, Pos_X, Pos_Y) = (2, 2.8, -0.1, 1)$ (unit: mm). Fig. 3 presents the simulation results of the parametric study conducted for these four variable parameters. The results indicate that the center resonant frequency of IMP-AiD Ver. 1 decreases as P_Y increases, while the overall wide bandwidth remains unchanged. This implies that the IMP stacked on the AiD FDA resonates at the observed center resonant frequency of IMP-AiD Ver. 1, while the additional lower and higher resonant frequencies originate from the AiD FDA but are reinforced by the impedance modulation of the IMP located near the AiD FDA. Furthermore, since the co-polarization of the FDA is y-polarization, the length of the IMP in the y-axis direction, P_Y, controls the center resonant frequency corresponding to the IMP resonance, whereas the width of the IMP in the x-axis direction, P_X, governs the impedance matching at the center resonant frequency.

Fig. 3(c) confirms that Pos_X has the most significant impact on bandwidth. When Pos_X is between −0.1 mm and −0.4 mm, Ver. 1 demonstrates a substantially wide bandwidth. Fig. 3(d) further illustrates that while Pos_Y influences impedance matching at the center resonant frequency, it has little effect on the overall bandwidth of IMP-AiD Ver. 1

Based on the results in Fig. 3(a), 3(b), and 3(d), the optimal values for P_X, P_Y, and Pos_Y were determined as 2 mm, 2.8 mm, and 1 mm, respectively, to maximize the impedance bandwidth of Ver. 1. However, since the −10 dB impedance bandwidth for Pos_X was nearly identical between −0.1 mm and −0.4 mm, further optimization of Pos_X was required. To achieve this, the peak realized gain with regard to frequency was analyzed. The results in Fig. 4 indicate that with $Pos_X = -0.1$ mm, IMP-AiD Ver. 1 achieves a −1 dB gain bandwidth of 10.0% (30.16–33.33 GHz), which is significantly wider than the other options with gain bandwidths of 7.3%, 5.1%, and 5.8%. Consequently, Pos_X was set to −0.1 mm.

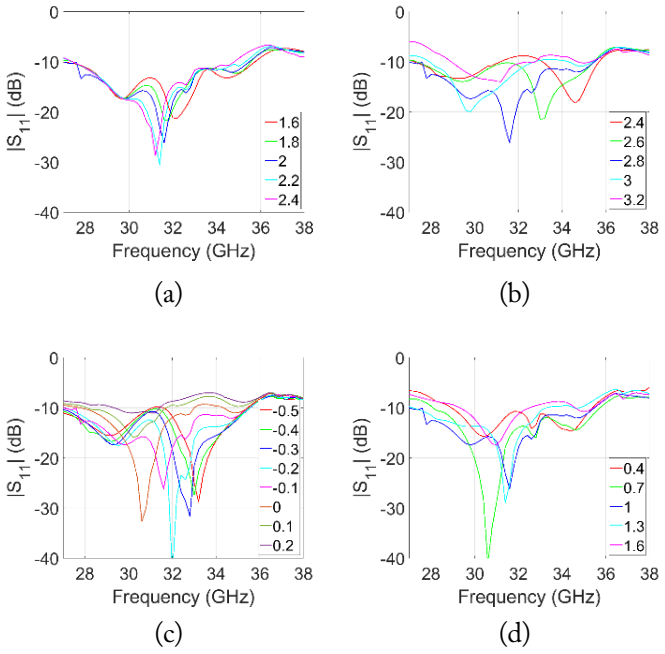

Fig. 3. $|S_{11}|$ simulation results of the parametric study for the wideband IMP-AiD (Ver. 1): (a) P_X, (b) P_Y, (c) Pos_X, and (d) Pos_Y. The default values are (P_X, P_Y, Pos_X, Pos_Y)=(2,2.8,−0.1,1) (unit: mm).

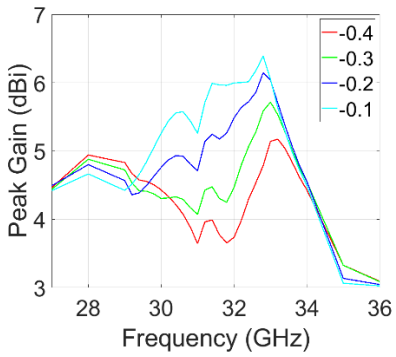

Fig. 4. Peak realized gain simulation results of the Pos_X parametric study for the wideband IMP-AiD (Ver. 1).

Fig. 5 illustrates the structure of the optimized IMP-AiD Ver. 1 and presents its simulated $|S_{11}|$ and peak realized gain pertaining to three different configurations: solid IMP, mesh-grid (optically transparent) IMP, and a realistic display size of 70 mm × 150 mm. The results confirm that IMP-AiD Ver. 1 maintains almost identical bandwidth regardless of whether a mesh-grid IMP or a large display is employed. When embedded in a realistic display, IMP-AiD Ver. 1 demonstrates a wide bandwidth of 26.3% (27.26–35.52 GHz), while the peak gain decreases to 5.48 dBi at 32.0 GHz. On the other hand, the −1 dB gain bandwidth increases to 15.3% (28.44–33.15 GHz), aligning well with the objective of designing a wideband-type IMP-AiD.

Fig. 6 illustrates the current distribution of the designed wideband IMP-AiD Ver. 1 at representative operating frequencies of 28, 31, and 34 GHz. It is evident that the proposed IMP-AiD Ver. 1 radiates with y-polarization across a wide operating bandwidth, maintaining co-polarization with the AiD-FDA. This further confirms the satisfactory wideband performance of the proposed design.

IV. Ver. 2: High Gain IMP-AiD Design

In this section, we present another type of IMP-AiD that is designed to achieve high gain at 30 GHz through gain control by adjusting the IMP parameters. In this design, referred to as Ver. 2, different values are assigned to variable parameters P_X, P_Y, Pos_X, and Pos_Y compared to IMP-AiD Ver. 1. For ease of application, the values of P_X, P_Y, and Pos_X were kept identical to those used in IMP-AiD Ver. 1, while Pos_Y was modified for the high-gain IMP-AiD Ver. 2. Specifically, the parameters were set as follows: (P_X, P_Y, Pos_X, Pos_Y) = (2, 2.8, 0.1, 1) (unit: mm).

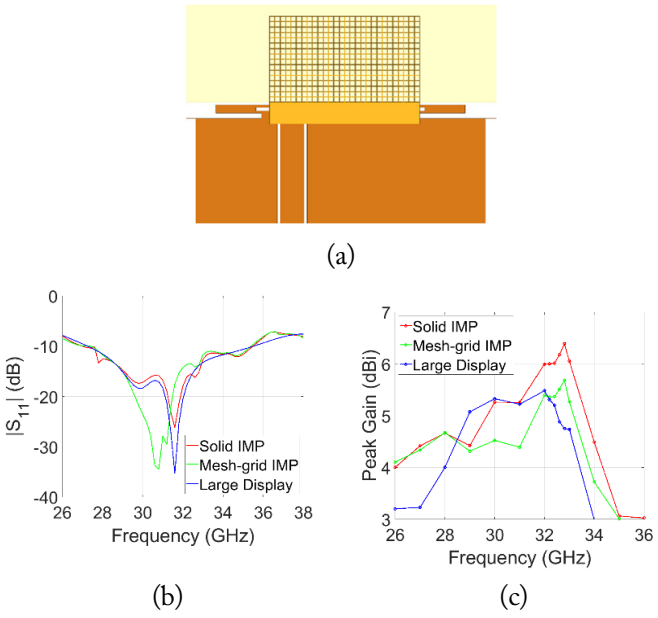

Fig. 5. (a) Configuration of IMP-AiD Ver. 1; (b) $|S_{11}|$ simulation results and (c) peak realized gain simulation results for IMP-AiD Ver. 1 when using a solid IMP, a mesh-grid IMP, and a realistic display size of 70 mm × 150 mm.

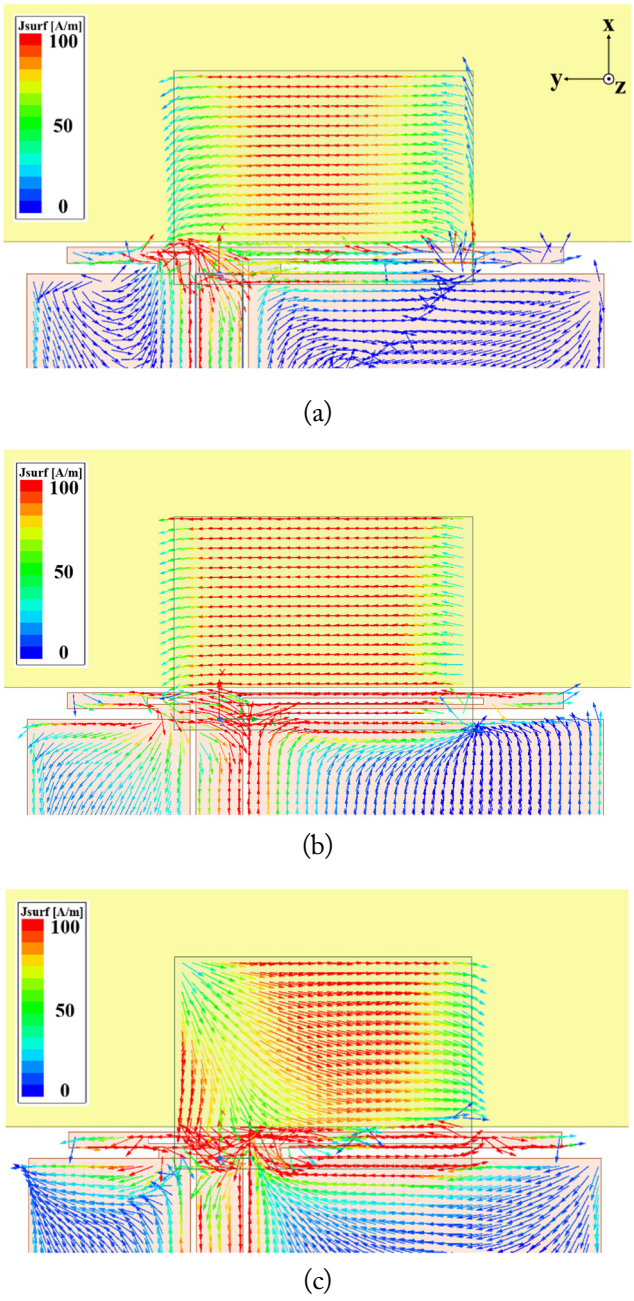

Fig. 6. Current distribution patterns of the wideband IMP-AiD (Ver. 1) at (a) 28 GHz, (b) 31 GHz, and (c) 34 GHz.

Fig. 7 shows the simulation results of the parametric study conducted to obtain the peak realized gain with regard to the frequency for the four variable parameters. The results indicate that P_Y primarily affects the peak gain at the target frequency (30 GHz). Furthermore, since Pos_X was fixed at 0.1 mm, only one resonance remains within the bandwidth, while the resonant frequency shifts as P_Y changes. This behavior can be attributed to IMP resonance.

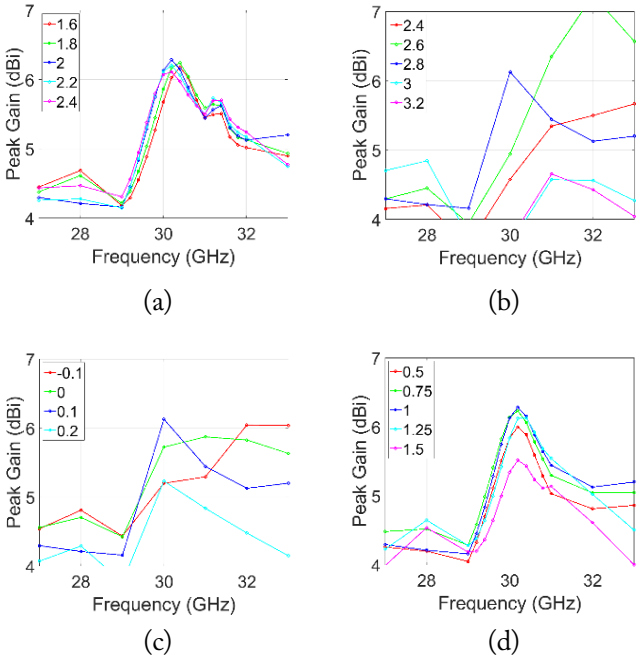

Fig. 7. Peak realized gain simulation results of the parametric study for the high-gain IMP-AiD (Ver. 2): (a) P_X, (b) P_Y, (c) Pos_X, and (d) Pos_Y. The default values are (P_X, P_Y, Pos_X, Pos_Y)=(2,2.8,0.1,1) (unit: mm).

Fig. 8 shows the structure of the optimized IMP-AiD Ver. 2, along with its simulated $|S_{11}|$ and peak realized gain for three configurations: solid IMP, mesh-grid (optically transparent) IMP, and a realistic display size of 70 mm × 150 mm. The three configurations exhibit similar bandwidths. Furthermore, when embedded in a realistic display, IMP–AiD Ver. 2 demonstrates a moderate bandwidth of 13.2% (27.97–31.91 GHz). Additionally, it achieves a peak gain of 6.25 dBi, with a −1 dB gain bandwidth of 5.7% (29.61–31.34 GHz).

Fig. 9 illustrates the current distribution of the designed high-gain IMP-AiD Ver. 2 at its center operating frequency of 30 GHz. It is evident that the proposed IMP-AiD Ver. 2 radiates with y-polarization across the operating bandwidth, maintaining co-polarization with the AiD-FDA. Notably, compared to IMP-AiD Ver. 1, more concentrated y-polarized surface currents are observed on both the IMP and AiD in the case of IMP-AiD Ver. 2, indicating the high-gain characteristics of the proposed design.

Fig. 10 compares the simulated $|S_{11}|$ and peak realized gain achieved for the AiD FDA without an IMP, as well as for IMP-AiDs Ver. 1 and Ver. 2. The results reveal that the AiD FDA without an IMP exhibits limited bandwidth and low peak gain. In contrast, by appropriately positioning the IMP with optimized dimensions over the AiD FDA at different relative locations, the gain and bandwidth of the IMP-AiD are successfully controlled. Specifically, Ver. 1 was optimized for a wide bandwidth, and Ver. 2 was optimized for high gain. Table 1 summarizes the gain and bandwidth characteristics of the AiD FDA and the two IMP-AiD designs.

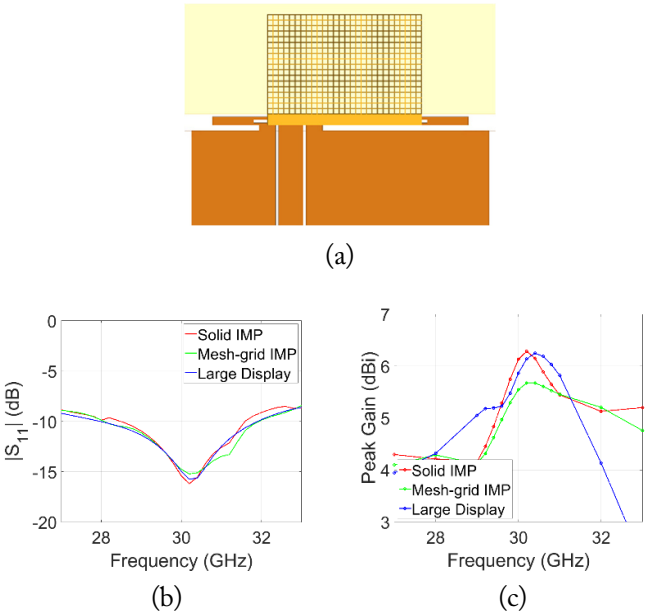

Fig. 8. (a) Configuration of IMP-AiD Ver. 2; (b) $|S_{11}|$ simulation results and (c) peak realized gain simulation results for IMP-AiD Ver. 2 with a solid IMP, a mesh-grid IMP, and a realistic display size of 70 mm × 150 mm.

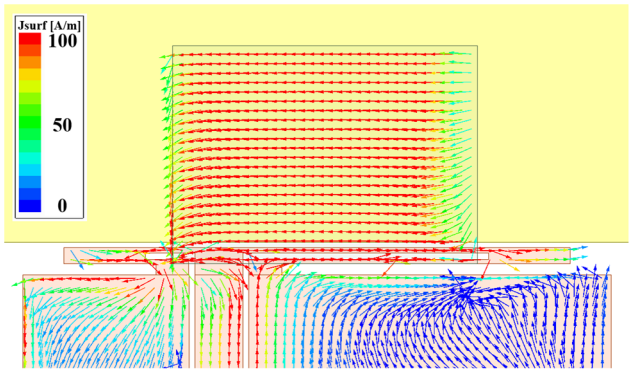

Fig. 9. Current distribution patterns of the high gain IMP-AiD (Ver. 2) at 30 GHz.

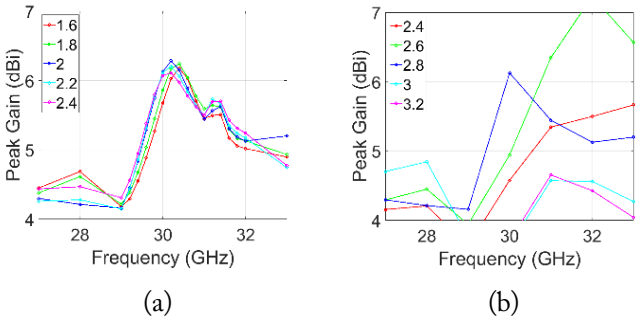

Fig. 10. (a) $|S_{11}|$ and (b) peak realized gain simulation results for the AiD-FDA without an IMP, as well as for Ver. 1 and Ver. 2 IMP-AiDs with a realistic display size of 70 mm × 150 mm.

Table 1. Comparison of the AiD-FDA without an IMP and the proposed IMP-AiDs

Parameter	AiD-FDA	IMP-AiD	
		Ver. 1	Ver. 2
Frequency (GHz)	30	32	30
Gain (dBi)	3.76	5.48	6.25
−10 dB $\|S_{11}\|$ bandwidth (%)	N/A	26.3	13.2
−1 dB gain bandwidth (%)	>20.0	15.3	5.7

V. Equivalent Circuit Model of IMP-AiDS

To examine the modulation of the operating bandwidth in IMP-AiDs Ver. 1 and Ver. 2, equivalent circuit modeling (ECM) was implemented. The physical nodes A–F on the AiD-FDA and C'–F' on the IMP used for ECM, as well as the schematic layouts for the ECM, are depicted in Fig. 11. The corresponding parameter values for IMP-AiDs Ver. 1 and Ver. 2 are listed in Table 2. Notably, the physical nodes C–F on the AiD-FDA and

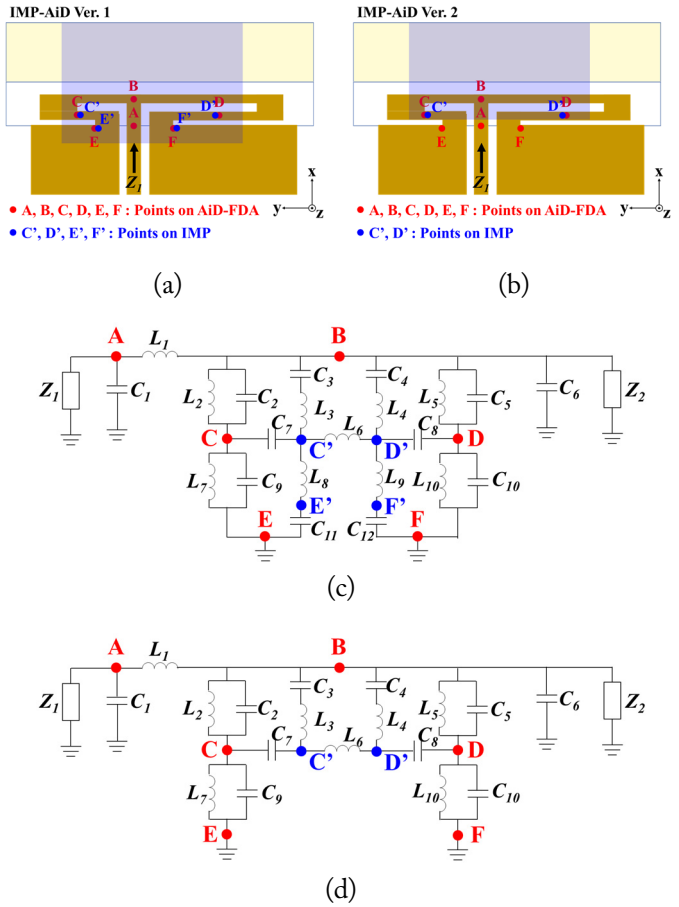

Fig. 11. Demonstration of the physical nodes A–F on AiD-FDA and C'–F' on IMP for equivalent circuit modeling (ECM) of (a) IMP-AiD Ver. 1 and (b) IMP-AiD Ver. 2; schematic layouts for the ECM of (c) IMP-AiD Ver. 1 and (d) IMP-AiD Ver. 2.

Table 2. Parameter values of the ECM for IMP–AiDs Ver. 1 and Ver. 2 corresponding to the configurations shown in Fig. 11(c) and 11(d)

Parameter	Value	Parameter	Value
Z_1	50	L_2	0.612
Z_2	377	L_3	0.05
C_1	29.02	L_4	0.01
C_2	63.3	L_5	0.525
C_3	1 (Ver. 1) 77.2 (Ver. 2)	L_6	0.181 (Ver. 1) 0.392 (Ver. 2)
C_4	3 (Ver. 1) 2.62 (Ver. 2)	L_7	0.25
C_5	76.82	L_8	0.259
C_6	0.1	L_9	0.05
C_7	240 (Ver. 1) 232.0 (Ver. 2)	L_{10}	0.57
C_8	120 (Ver. 1) 218.7 (Ver. 2)	R_{L1}	5.86
C_9	75.6	R_{L2}	25.94
C_{10}	104.4	R_{L5}	30
C_{11}	88.41	R_{L6}	0.05
C_{12}	118.83	R_{L7}	6.22
L_1	0.453	R_{L10}	30

The units of parameters are used in nH, fF, and Ω.

C'–F' on the IMP, which are observed to be aligned in the top view, are actually vertically displaced, with capacitance present in between. In addition, capacitances C_3 and C_4, and inductances L_3, L_4, and L_6, are located between the physical nodes B, C', and D'. As shown in the schematic layouts, the capacitances and inductances surrounding nodes E' and F' are eliminated when the IMP in IMP-AiD Ver. 1 is shifted along the x-axis to form IMP-AiD Ver. 2 since they become negligible. This change critically affects the operating bandwidth of the IMP-AiDs because the number of resonances varies based on the existence or varying values of the capacitances and inductances associated with the horizontal position of the IMP. Fig. 12 shows that the $|S_{11}|$ values simulated using ECM are in good agreement with those obtained from HFSS simulations for both IMP-AiDs Ver. 1 and Ver. 2.

VI. Experimental Results and Discussion

1. Fabrication and Measurement

To validate the simulation results, one of the demonstrated IMP-AiDs—the high-gain type IMP-AiD (Ver. 2)—was fabricated and measured. The fabrication process involved manual ad-

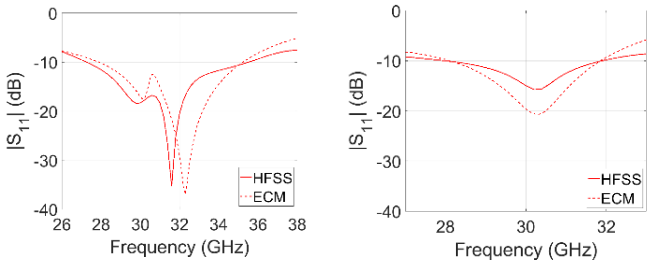

Fig. 12. HFSS-simulated and ECM-simulated $|S_{11}|$ of (a) IMP-AiD Ver. 1 and (b) IMP-AiD Ver. 2.

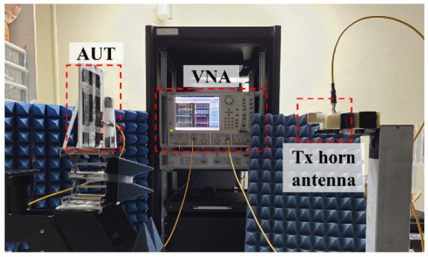

Fig. 13. Photograph of the measurement setup for the display-integrated Ver. 2 IMP-AiD.

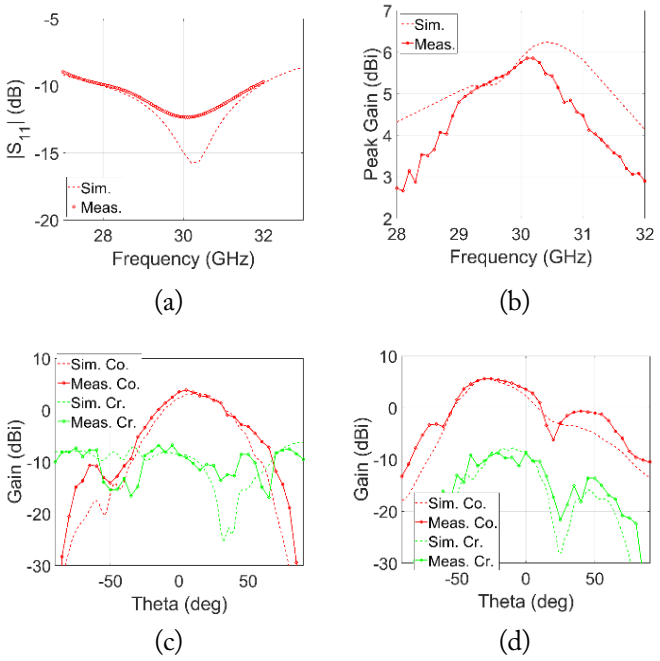

Fig. 14. Simulated and measured (a) $|S_{11}|$, (b) peak gain over frequency, (c) E-plane radiation pattern and (d) H-plane radiation pattern at 30.1 GHz for IMP-AiD Ver. 2.

hesion of the display layers and COP film using a microscope, as detailed in [16]. Fig. 13 shows the measurement setup for the display-integrated IMP-AiD Ver. 2. Notably, as shown in Fig. 2(b), the fabricated sample achieved a high optical transparency (OT) of 89% based on the assigned W_{cell} and W_{mesh} values [13].

Fig. 14 shows the simulated and measured $|S_{11}|$, peak realized gain in terms of frequency, and E- and H-plane radiation patterns of IMP-AiD Ver. 2. The simulated and measured results largely show good agreement, with the measured -10 dB impedance bandwidth of 12.4% (28.1–31.8 GHz) closely matching the corresponding simulated result. Furthermore, the measured peak gain is 5.86 dBi at 30.1 GHz, which is 0.39 dB lower than the simulated value, while the measured -1 dB gain bandwidth is 6.0% (29.0–30.8 GHz), also consistent with the simulation result. Additionally, the simulated and measured E- and H-plane radiation patterns at 30.1 GHz, where peak gain occurs, demonstrate good agreement. The minor discrepancies between the simulation and measurement results can be attributed to alignment errors during the manual fabrication process.

As shown in Fig. 14(c) and 14(d), the cross-polarization discrimination (XPD) is 13.0 dB and 15.9 dB along the main beam direction in the E- and H-planes, respectively. Additionally, the radiation efficiency at 30.1 GHz was calculated to be 59.8%, which was obtained by dividing the measured gain by the simulated directivity, as explained in [5].

2. Performance Comparison and Discussion

Table 3 compares the proposed IMP-AiDs with conventional display antennas. By integrating a gain- and bandwidth-controllable IMP into the AiD dipole antenna, the wide-bandwidth type IMP-AiD Ver. 1 achieved the widest impedance bandwidth among the AoDs and AiD, while also exhibiting a higher gain than both. Similarly, the high-gain type IMP-AiD Ver. 2 achieved the highest gain among the AoDs and AiD, as well as a wider bandwidth than those reported in [5] and [17]. Furthermore, the radiation efficiencies of IMP-AiDs Ver. 1 and Ver. 2 are either comparable to or exceed the typical radiation efficiency range of 50%–70% that is commonly observed in AoDs and AiDs.

One may question the compatibility of the IMP with the touch sensor panel (TSP), given that they overlap in certain areas. However, similar challenges have been addressed for AoD patch antennas, which also overlap with the TSP. Although AoD patches cover only a part of the TSP, previously published research papers [18] and patents [19, 20] offer technical solutions to mitigate this issue. For instance, this challenge can be addressed by positioning the patch on the Tx electrode of the TSP and incorporating an insulating layer between the TSP-sensing electrodes and the patches. Similarly, the IMP proposed in our manuscript can be easily integrated into the display panel and can also contribute to minimizing TSP degradation, making it suitable for mmWave smartphones.

VII. Conclusion

This paper proposes a novel display antenna scheme that integrates an IMP with a pre-printed AiD FDA positioned at the

Table 3. Comparison of the AiD FDA with conventional display antennas (single element)

	This work		Park et al. [5]	Lee et al. [9]	Oh et al. [17]
	Ver. 1	Ver. 2			
Scheme	IMP-AiD	IMP-AiD	AoD	AoD	AiD
Frequency (GHz)	32	30	28	28 / 38	28 / 28
Gain (dBi)	5.48	(Sim.) 6.25 (Meas.) 5.86	4.05	1.9 / 2.2	3.56 / 3.1
−10 dB $\|S_{11}\|$ bandwidth (%)	26.3	12.4	2.3	17.8 / 19	6.2 / 9.2
−1 dB gain bandwidth (%)	15.3	6.0	NA	NA	NA
Radiation efficiency (%)	57.4	59.8	52.4	NA	NA

edge of the OLED panel. Although the AiD FDA, when fabricated together with the OLED panel, lacks performance diversity, its gain and bandwidth can be easily controlled—either to maximize bandwidth or gain—by simply adjusting the integration position of the IMP over the AiD FDA. IMP-AiDs Ver. 1 and Ver. 2 were fabricated, achieving the widest bandwidth and highest gain, respectively, compared to conventional display antennas, while also maintaining good gain and bandwidth, respectively.

Future studies on this topic should focus on automating the fabrication processes to minimize alignment errors, evaluating thermal and mechanical reliability when integrating radio-frequency integrated circuits (RFIC) into the proposed IMP-AiD, and expanding the equivalent circuit model validation over a broader frequency range.

This work was supported in part by Samsung Display and in part by the Korea Government Ministry of Science and ICT (MSIT) (No. RS-2021-II210763, Innovative Fusion Technologies of Intelligent Antenna Material/Structure/Network for THz 6G).

References

[1] H. C. Huang, "Evolution of millimeter-wave antenna solutions and designs to cellular phones," *IEEE Access*, vol. 8, pp. 187615-187622, 2020. https://doi.org/10.1109/ACCESS.2020.3027424

[2] B. Kim, S. Bang, S. Yun, H. Kim, and J. Oh, "Broadband holographic mode synthesis between adjacent resonances for a low-profile thin-microstrip antenna-fed metasurface," *IEEE Transactions on Antennas and Propagation*, vol. 73, no. 11, pp. 9577-9582, 2025. https://doi.org/10.1109/TAP.2025.3590571

[3] B. Kim and J. Oh, "Dual-wideband low-profile three-notch patch antenna with indirect differential feeding for 5G millimeter-wave applications," *IEEE Antennas and Wireless Propagation Letters*, vol. 24, no. 9, pp. 2734-2738, 2025. https://doi.org/10.1109/LAWP.2025.3572958

[4] B. Kim, J. Jung, S. Yun, H. Kim, and J. Oh, "Heterogeneous metasurface empowering proximate high-permittivity ceramic cover for a 5G dual-band millimeter-wave smartphone," *IEEE Transactions on Antennas and Propagation*, vol. 72, no. 5, pp. 4086-4094, 2024. https://doi.org/10.1109/TAP.2024.3383725

[5] J. Park, S. Y. Lee, J. Kim, D. Park, W. Choi, and W. Hong, "An optically invisible antenna-on-display concept for millimeter-wave 5G cellular devices," *IEEE Transactions on Antennas and Propagation*, vol. 67, no. 5, pp. 2942-2952, 2019. https://doi.org/10.1109/TAP.2019.2900399

[6] H. Qiu, H. Liu, X. Jia, Z. Y. Jiang, Y. H. Liu, J. Xu, et al., "Compact, flexible, and transparent antennas based on embedded metallic mesh for wearable devices in 5G wireless network," *IEEE Transactions on Antennas and Propagation*, vol. 69, no. 4, pp. 1864-1873, 2021. https://doi.org/10.1109/TAP.2020.3035911

[7] B. Kim and S. Hwangbo, "Optically transparent holographic display antenna: high gain, beam steering, and lossless bonding for 5G millimeter-wave n261 band," *IEEE Open Journal of Antennas and Propagation*, vol. 6, no. 6, pp. 1799-1814, 2025. https://doi.org/10.1109/OJAP.2025.3601621

[8] J. M. Heo, E. J. Sung, J. K. Kim, and G. Byun, "Characteristic impedance adjustment of thin-metal mesh transmission lines for mmWave display-integrated antennas," *IEEE Access*, vol. 9, pp. 94714-94722, 2021. https://doi.org/10.1109/ACCESS.2021.3094160

[9] D. Lee, B. Kim, J. Lee, Y. Youn, M. Kim, S. Chang, D. Park, and W. Hong, "Dual-polarized dual-band antenna-on-display using via-less and single-layer topology for mmWave wireless scenarios," *IEEE Antennas and Wireless Propagation Letters*, vol. 22, no. 5, pp. 1000-1004, 2023. https://doi.org/10.1109/LAWP.2022.3230469

[10] B. Kim and J. Oh, "Single-glass-layer optically transparent transmitarray with high aperture efficiency and low profile at 5G millimeter-wave band," *IEEE Transactions on Antennas and Propagation*, vol. 71, no. 11, pp. 9036-9041, 2023. https://doi.org/10.1109/TAP.2023.3305876

[11] B. Kim and J. Oh, "Characterization of optically transparent two-metal-layered refractive metasurfaces for 6G upper-mid outdoor-to-indoor communication," in *Proceedings of 2024 IEEE International Symposium on Antennas and Propagation and INC/USNC-URSI Radio Science Meeting (AP-S/INC-USNC-URSI)*, Firenze, Italy, 2024, pp. 1363-1364. https://doi.org/10.1109/AP-S/INC-USNC-URSI52054.2024.10686503

[12] B. Kim, S. Bang, S. Kim, D. Kwon, S. Kim, and J. Oh, "Locally optimal periods in periodic optically transparent two-metal-layered refractive metasurfaces for outdoor-to-indoor communication," *IEEE Antennas and Wireless Propagation Letters*, vol. 24, no. 5, pp. 1253-1257, 2025. https://doi.org/10.1109/LAWP.2025.3532301

[13] S. H. Kang and C. W. Jung, "Transparent patch antenna using metal mesh," *IEEE Transactions on Antennas and Propagation*, vol. 66, no. 4, pp. 2095-2100, 2018. https://doi.org/10.1109/TAP.2018.2804622

[14] K. K. So, B. J. Chen, and C. H. Chan, "Microwave and millimeter-wave MIMO antenna using conductive ITO film," *IEEE Access*, vol. 8, pp. 207024-207033, 2020. https://doi.org/10.1109/ACCESS.2020.3037900

[15] S. Hong, S. H. Kang, Y. Kim, and C. W. Jung, "Transparent and flexible antenna for wearable glasses applications," *IEEE Transactions on Antennas and Propagation*, vol. 64, no. 7, pp. 2797-2804, 2016. https://doi.org/10.1109/TAP.2016.2554626

[16] J. Oh, B. Kim, S. Yoon, K. Kim, E. J. Sung, and J. Oh, "High-gain millimeter-wave antenna-in-display using non-optical space for 5G smartphones," *IEEE Transactions on Antennas and Propagation*, vol. 71, no. 2, pp. 1458-1468, 2023. https://doi.org/10.1109/TAP.2022.3228912

[17] J. Oh, K. Kim, J. Choi, and J. Oh, "Tightly embedded modular antenna-in-display (MAiD) into the panel edge of display with dual-polarization for 5G smartphones," *IEEE Transactions on Antennas and Propagation*, vol. 73, no. 2, pp. 1209-1214, 2025. https://doi.org/10.1109/TAP.2024.3501415

[18] W. Hong, S. Lim, S. Ko, and Y. G. Kim, "Optically invisible antenna integrated within an OLED touch display panel for IoT applications," *IEEE Transactions on Antennas and Propagation*, vol. 65, no. 7, pp. 3750-3755, 2017. https://doi.org/10.1109/TAP.2017.2705127

[19] S. H. Lim, S. T. Ko, Y. G. Kim, and W. B. Hong, "Antenna device and electronic device having the same," US Patent 9652073B2, May 16, 2017.

[20] J. M. Kim, D. P. Park, and B. J. Choi, "Touch sensor including antenna," US Patent 10990234B2, April 27, 2021.

Byeongjin Kim
https://orcid.org/0000-0003-1667-5144

received his B.S. degree in electrical and computer engineering from Seoul National University, Korea, in 2020, where he is currently pursuing an integrated master's and Ph.D. degree. His current research interests include display antennas, antennas-in-package, optically transparent antennas, passive and reconfigurable transmitarrays and reflectarrays based on semiconductor process and liquid crystal, metasurface antennas, holographic metasurface antennas, FMCW radar systems, and ray-tracing for 5G millimeter-wave, 6G upper-mid, and 6G sub-terahertz (THz) communication and sensing systems.

Jeongtaek Oh
https://orcid.org/0000-0002-8446-2194

received his B.S. degree in electrical and computer engineering from Seoul National University, Korea, in 2020, where he is currently pursuing an integrated master's and Ph.D. degree. His current research interests include display antennas and metamaterial-based transmitarray antennas for mmWave communication systems.

Kiseo Kim
https://orcid.org/0009-0005-1283-981X

received his Master of Science degree in physics from Kyung Hee University, Seoul, South Korea, in 2008. He is currently an engineer with Samsung Display. His research interests include display integrated antennas and next-generation displays.

Jungsuek Oh
https://orcid.org/0000-0002-2156-4927

received his B.S. and M.S. degrees from Seoul National University, Korea, in 2002 and 2007, respectively, and a Ph.D. degree from the University of Michigan at Ann Arbor in 2012. From 2007 to 2008, he was with Korea Telecom as a hardware research engineer, working on the development of flexible RF devices. In 2012, he was a postdoctoral research fellow in the Radiation Laboratory at the University of Michigan. From 2013 to 2014, he was a staff RF engineer with Samsung Research America, Dallas, working as a project leader for the 5G/millimeter-wave antenna system. From 2015 to 2018, he was a faculty member in the Department of Electronic Engineering at Inha University in South Korea. He is currently a full Professor with tenure in the School of Electrical and Computer Engineering, Seoul National University, South Korea. His research areas include mmWave beam focusing/shaping techniques, antenna miniaturization for integrated systems, radio propagation modeling for complex environments, and AI based RF/EM system simulators. He is the recipient of the 2011 Rackham Predoctoral Fellowship Award at the University of Michigan. His group has been recognized with numerous awards at leading academic and industrial conferences. He has published more than 200 technical journal and conference papers, and has served as a TPC member and as a session chair for the IEEE AP-S/USNC-URSI, ISAP and APMC. He has been a senior member of IEEE since 2017.